Journal of Power Sources 372 (2017) 260–269

Contents lists available at ScienceDirect

Journal of Power Sources

journal homepage: www.elsevier.com/locate/jpowsour

Ultra-facile fabrication of phosphorus doped egg-like hierarchic porous carbon with superior supercapacitance performance by microwave irradiation combining with self-activation strategy

Deyi Zhang[a,b,c,*], Mei Han[b], Yubing Li[b], Jingjing He[b], Bing Wang[b], Kunjie Wang[b], Huixia Feng[b]

[a] State Key Laboratory of Advanced Processing and Recycling of Nonferrous Metals, Lanzhou University of Technology, Lanzhou 730050, China
[b] College of Petrochemical Technology, Lanzhou University of Technology, Lanzhou 730050, China
[c] Key Laboratory of Eco-Environment-Related Polymer Materials of Ministry of Education, Northwest Normal University, Lanzhou 730070, China

HIGHLIGHTS

- An ultra-facile method was developed for fabricating phosphorus doped egg-like HPC.
- The reported method exhibits incomparable merits comparing with the traditional method.
- Carbonization and self-activation process finish in 3 min under air atmosphere.
- Capacitance retention rate reaches 96.2% as current density increasing to 20 A g^{-1}.

GRAPHICAL ABSTRACT

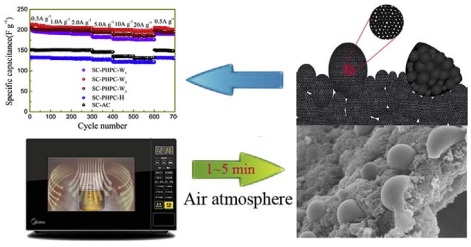

ARTICLE INFO

Keywords:
Microwave irradiation
Self-activation
Supercapacitor
Hierarchic porous carbons
Phosphorus doping

ABSTRACT

Herein, we report an ultra-facile fabrication method for a phosphorus doped egg-like hierarchic porous carbon by microwave irradiation combining with self-activation strategy under air atmosphere. Comparing with the traditional pyrolytic carbonization method, the reported method exhibits incomparable merits, such as high energy efficiency, ultra-fast and inert atmosphere protection absent fabrication process. Similar morphology and graphitization degree with the sample fabricated by the traditional pyrolytic carbonization method under inert atmosphere protection for 2 h can be easily achieved by the reported microwave irradiation method just for 3 min under ambient atmosphere. The samples fabricated by the reported method display a unique phosphorus doped egg-like hierarchic porous structure, high specific surface area (1642 m^2 g^{-1}) and large pore volume (2.04 cm^3 g^{-1}). Specific capacitance of the samples fabricated by the reported method reaches up to 209 F g^{-1}, and over 96.2% of initial capacitance remains as current density increasing from 0.5 to 20 A g^{-1}, indicating the superior capacitance performance of the fabricated samples. The hierarchic porous structure, opened microporosity, additional pseudocapacitance, high electrolyte-accessible surface area and good conductivity make essential contribution to its superior capacitance performance.

1. Introduction

How to significantly reduce the cost of high-performance electrochemical energy storage (EES) devices is a key challenge for the advancement of electrical vehicles and renewable energy [1,2]. The cost of the EES devices mainly dependents on price of electrode materials [3], so it is extremely important to develop cost-efficient electrode materials without sacrificing high performance. Currently, various

* Corresponding author. State Key Laboratory of Advanced Processing and Recycling of Nonferrous Metals, Lanzhou University of Technology, Lanzhou 730050, China.
E-mail address: lzdeyizhang@163.com (D. Zhang).

http://dx.doi.org/10.1016/j.jpowsour.2017.10.082
Received 24 August 2017; Received in revised form 9 October 2017; Accepted 25 October 2017
Available online 05 November 2017
0378-7753/

carbons are dominant electrode materials for EES devices, such as lithium-ion batteries (mainly for anode) and electrochemical supercapacitors, due to large specific surface area, good electrical conductivity, excellent physical and chemical stability, and environmental friendliness [4–6]. Many novel carbon materials, such as graphene, carbon nanotube, hollow carbon shell and ordered mesoporous carbon, exhibit excellent energy storage capability, and are suggested to use as electrode materials for high-performance EES devices [4], but the high cost of these materials obstructs their practical application. Alternatively, low-cost porous carbons (PCs), especially for activated carbon (AC), attracts constant attention of researchers and engineers, and have been extensively applied in commercial EES devices [5,7,8].

However, commercial high-quality porous carbons for energy storage application still have two main bottlenecks: a tedious and highly energy intensive fabrication process, and low energy density, which significantly limit their broad application [9]. The cost advantage of PCs comparing with other carbon materials mainly bases on the cheap and easily accessible raw materials [3]. Biomass and industrial wastes, such as egg white, seaweed, rice husk, honeysuckle, oily sludge, etc., can be readily utilized for fabricating porous carbons [10–14]. However, a carbonization process at high temperatures (600–1000 °C) for 1–4 h under a protection of inert atmosphere is necessary for fabricating porous carbons by using above raw materials, energy utilization efficiency in that process is intolerable low, and the necessary inert atmosphere protection makes fabrication condition rigorous. Furthermore, various activators, such as KOH, $ZnCl_2$ or phosphoric acid, are used to get high porosity and large surface area utilizing the chemical reaction between activators and carbon under high temperatures, which causes low convert ratio of raw materials and tedious post-treatment process [10,11]. Comparing with the traditional pyrolytic carbonization, microwave heating converses energy by dipole rotation and ionic conduction inside the substances which inducing temperatures of up to 1000 °C within just few minute [15], so microwave irradiation is regarded as a fascinating and promising tool for preparation of porous carbon material [15–21]. However, due to the poor microwave adsorption for most of carbonaceous material, in the first stage, the carbonaceous precursor, such as coconut shells or pineapple peel, is pyrolized under an inert atmosphere, and then the carbonized production is impregnated with an activation agent, e.g., KOH or K_2CO_3, followed by a microwave-induced chemical activation under an inert atmosphere [17–19]. Alternatively, porous carbons also can be facilely obtained by a simple one-step microwave treatment of the activation agent/microwave absorber impregnated precursor under or without the protection of inert atmosphere. For instance, Eder C. Lima et al. obtained an activated carbon with a specific surface area of up to 619 $m^2\ g^{-1}$ by microwave irradiating a mixture of cocoa shell and inorganic components (lime + $ZnCl_2$ + $FeCl_3$) for about 10 min under nitrogen [20]. Ali U. Shaikh et al. reported a heteroatom doped mesoporous carbon with a specific surface area of 855 $m^2\ g^{-1}$ synthesized by microwave irradiating tannin cross-linked melamine for 30 min using polyphosphoric acid as microwave absorber and activation agent under ambient atmosphere [15,21]. As far as our knowledge, there are rare studies on the one-step fabrication of porous carbons by microwave irradiation combining with self-activation under air atmosphere.

The relatively low energy density of porous carbons comparing with other carbon electrode materials is mainly due to poor electrolyte accessibility caused by the micropores dominant pore structure [22]. Fortunately, the research conducted by Y. Gogotsi et al. revealed that electrolyte accessibility of micropores can be efficiently improved by constructing short opened micropores [23], which provides an efficient strategy for enhancing the energy density of PCs. Thus, the hierarchical porous carbon with short opened micropores connected to mesopores and macropores is extensively exploited as high-performance electrode material for EES application [24,25]. For example, a hierarchical porous carbon microtube with a specific surface area of 1775.7 $m^2\ g^{-1}$ derived from willow catkins exhibited a high capacitance of 292 F g^{-1} at a current density of 1 A g^{-1} in 6 M KOH aqueous solution, and a high energy density of 37.9 Wh kg^{-1} at a power density of 700 W kg^{-1} in 1 M $LiPF_6$ electrolyte [26]. Recently, Junke Ou et al. also reported a hierarchical porous carbon with opened micropores derived from honeysuckle, which reversible capacity reached up to 1215 mAh g^{-1} at a current density of 100 mA g^{-1} when used as an anode of lithium-ion batteries [12]. Furthermore, recent researches indicated that the heteroatoms doping, such as N, S and P doping, could be another efficient strategy for improving the electrolyte accessibility of micropore and small mesopore. The difference in electronegativity between the heteroatoms and host C atoms provides a more polarized surface, which consequentially promoting the wettability of the carbon surface and thus ensures a fast transfer rate of electrolytic ions in micropores and small mesopores, and finally improves their electrolyte accessibility [25,27,28]. The improved electrolyte accessibility enhances the utilization ratio of micropores and small mesopores, thus improves the energy storage/release capability of porous carbons. So a dramatic improvement for energy density of porous carbons by combining heteroatoms doping with hierarchical porous structure is reasonable to expect [15,25].

In this work, we report an ultra-facile fabrication method for a phosphorus doped egg-like hierarchic porous carbon by microwave irradiation combining with self-activation strategy under air atmosphere using phytic acid as precursor. Comparing with the traditional pyrolytic carbonization method, the reported method exhibits incomparable merits, such as high energy utilization efficiency, absence of inert atmosphere protection and ultra-fast fabrication process. The samples fabricated by the reported method with high specific surface area (up to 1642 $m^2\ g^{-1}$) and developed opened microporosity exhibit a superior capacitance performance when used as an electrode material for symmetric supercapacitor cell, which specific capacitance reaches up to 209 F g^{-1} at a current density of 0.5 A g^{-1}, and over 96.2% of initial capacitance remains as the current density increasing to 20 A g^{-1}.

2. Experiment

2.1. Fabrication of the phosphorus doped egg-like hierarchic porous carbons by a microwave irradiation combining with self-activation strategy

The phosphorus doped egg-like hierarchic porous carbon was facilely fabricated by a microwave irradiation combining with self-activation strategy using phytic acid as precursor under an air atmosphere. The general fabrication process is summarized and illustrated in Fig. 1. Briefly, 5 g of the phytic acid solution (50% w/w in H_2O, Sigma) was directly microwave irradiated in a household microwave oven (M1-231A, Midea, China) under a radiation power of 800 W for 1–5 min, followed by washing with deionized water and drying under a radiation power of 500 W in microwave oven for 2 min. The final product refers to as PHPC-W_x, where x denotes the microwave irradiation time.

2.2. Fabrication of the phosphorus doped egg-like hierarchic porous carbon by traditional pyrolytic carbonization

For demonstrating the advantages of the method presented above, a phosphorus doped egg-like hierarchic porous carbon was also fabricated by traditional pyrolytic carbonization. In brief, 5 g of the phytic acid solution (50% w/w in H_2O, Sigma) was directly carbonized in a tube furnace under 650 °C for 2 h with the protection of argon atmosphere, followed by washing with deionized water and drying at 105 °C for 12 h. The final product refers to as PHPC-H.

Furthermore, a commercial AC (yp-50F) with a specific surface area of 1687 $m^2\ g^{-1}$ purchased from Kurary Co., Ltd.(Japan) was used to compare the capacitance performance with the reported phosphorus doped egg-like hierarchic porous carbon.

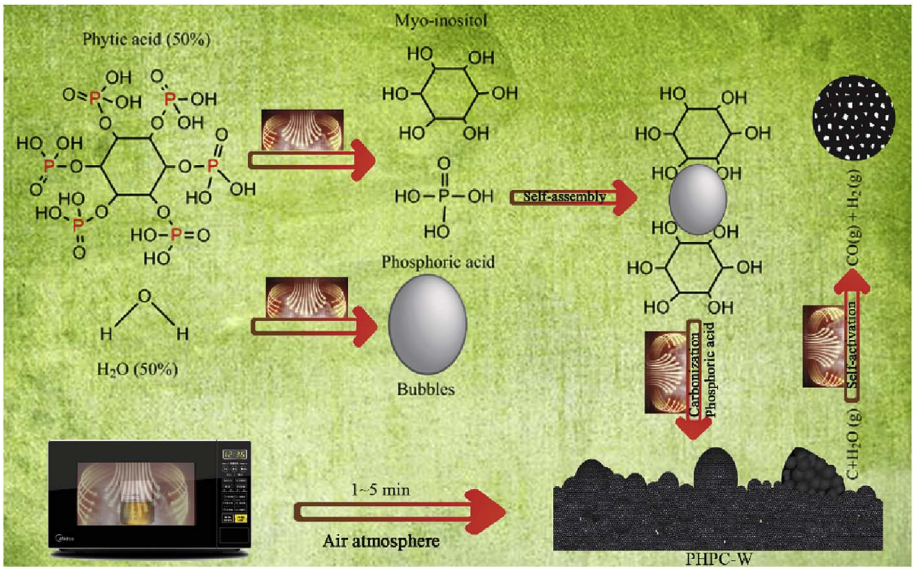

Fig. 1. Scheme for the fabrication of PHPC-W.

2.3. Electrochemical measurements

The capacitance performance of the fabricated samples and commercial AC was evaluated in 6 M KOH in a three-electrode configuration and two-electrode symmetric cell. The work electrode were prepared by coating the slurry containing active materials (80 mw%), acetylene black (10 mw%) and polytetrafluoroethylene (PTFE, 10 mw %) onto a nickel foam with a size of 1.2 cm × 1.2 cm, and pressing under 10 MPa for 1 min. The electrode plates were then dried in a vacuum at 110 °C for 24 h. The thickness of each electrode was ca. 0.1 mm, and the total mass for each electrode was ca. 4.2 mg. In a conventional three-electrode configuration, a patinum foil with a size of 1.0 cm × 1.0 cm and an Ag/AgCl electrode were used as the counter and reference electrode, respectively. For the two-electrode symmetric supercapacitors, CR2032-type coin cells were assembled by sandwiching of the separator (PP/PE complex film) between two identical electrodes. Cycling voltammetry (CV) curves within a potential range of −1.0 ~ 0V for three-electrode configuration and 0–1.0V for the assembled two-electrode symmetric cells were obtained using a CHI660E electrochemical workstation. Electrochemical impedance spectroscopies (EIS) conducted in the frequency range of 100 kHz to 0.1 Hz with ac amplitude of 5 mV and self-discharge characteristic of the assembled two-electrode symmetric cells also were performed on a CHI660E electrochemical workstation, while the galvanostatic charging-discharging curves, leakage current and cycle-life stability of the assembled two-electrode symmetric cells were tested using a computer controlled supercapacitor testing system (NEWARE, Shenzhen China) within a potential range of 0–1.0V.

2.4. Characterization

Surface morphology of the reported materials were measured using a Hitachi S4800 field emission scanning electron microscope (FESEM, Japan) and a JEOL JEM-2010 transmission electron microscopy (TEM, Japan). X-ray photoelectron spectra (XPS) was collected on an Escalab 250Xi spectrometer (Thermo Scientific, USA), using a monochromatized Al Kα X-ray source. Raman spectra was measured on a Horiba JY-HR800 Raman microscope (Japan) with an excitation wavelength of 532 nm. Nitrogen adsorption and desorption isotherms were performed using a Micromeritics ASAP 2460 automatic analyzer (USA). Samples were degassed at 200 °C for 12 h prior to the measurement. The total specific surface area (S_{BET}) was calculated by the BET method using the N_2 adsorption data. Meanwhile, the surface area, pore volume and according pore size distributions for mesopore and macropore were calculated by the Barrett − Joyner − Halenda (BJH) method, while the Horvath-Kawazoe (H-K) model was employed to evaluate the surface area, pore volume and according pore size distributions of micropore. Thermogravimetric and differential thermal analysis (TG-DTA) was conducted on a Netzsch STA449C thermogravimetric analyzer under an argon atmosphere with a heating temperature range of 25–900 °C, and the heating rate was controlled at 20 °C min^{-1}.

3. Results and discussion

The scheme for the fabrication of phosphorus doped egg-like hierarchic porous carbon by microwave irradiation combining with self-activation strategy is suggested on Fig. 1. Microwave energy can be readily transformed into heat inside the particles by dipole rotation and ionic conduction [29]. Under the microwave irritation, the temperature of reaction system rapidly increases due to the strong microwave adsorption of strong polar phytic acid and H_2O molecules. The water in reaction system is gasified instantaneously, and forms little egg-like bubbles in the high-viscosity phytic acid solution due to strong hydrogen-bond effect between phytic acid and H_2O molecules. Phytic acid molecules continuously decompose to myo-inositol and phosphoric acid with the sharply increasing temperature [30,31]. Under the effect of strong hydrogen-bond, myo-inositol molecules self-assemble on the surface of bubbles, and then carbonize by intramolecular dehydration to form “egg-shell” when the temperature of reaction system is high enough. Meanwhile, phosphoric acid molecules self-polymerize to form pyrophosphoric acid, and finally form polyphosphoric acid by intramolecular dehydration with the sharply increasing temperature [31,32]. Pyrophosphoric acid and its derivatives are good microwave absorber with high thermostability [15,21], especially for polyphosphoric acid which boiling point achieves 856 °C. The ultra-high boiling point of polyphosphoric acid ensures the temperature of reaction system can be heated to higher than 800 °C. Meanwhile, pyrophosphoric acid and its derivatives restrain the contact of carbonized productions of precursor with air, it allows the fabrication process can be conducted under an air atmosphere. As the temperature is high enough, the high temperature water steam sealed in “egg-shell” reacts with the “egg-shell” by the following reaction equation to form short opened micropores in the “egg-shell” [19,33].

$$C(s) + H_2O(g) \rightarrow CO(g) + H_2(g) \quad (1)$$

The TG-DTA test provides a direct proof for the pore and

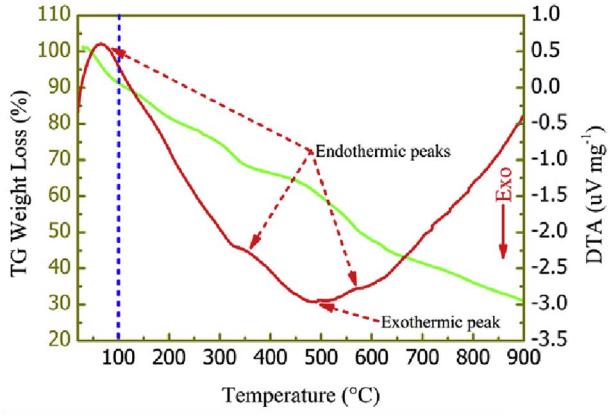

Fig. 2. TG-DTA curve of phytic acid.

morphology evolution speculated on Fig. 1. As show in Fig. 2, a continuous weight loss is observed as the temperature increasing from 25 to 900 °C for phytic acid solution (50% w/w in H_2O). The initial weight loss accompanying by apparently endothermic peak as the temperature increasing to 100 °C corresponds to the evaporation of water. Interestingly, this weight loss is no more than 10% of the total reactant mass although the mass concentration of water is near 50%, indicating that the most of water is retained in the reaction system even the temperature is higher than boiling point of water, and continuously escapes from the reaction system during the whole heating process. The strong hydrogen-bond interaction between the phytic acid and H_2O molecules hinders the escape of water vapor from reaction system, which then form egg-like bubbles in the high-viscosity phytic acid solution as the temperature is higher than 100 °C. With the increasing temperature, a continuously exothermic hydrolysis process referring to decomposition reaction of phytic acid to myo-inositol and phosphoric acid can be observed [34–36]. The huge exothermic peak centered at 490 °C is ascribed to the carbonization process of myo-inositol by intramolecular dehydration catalyzed by phosphoric acid and its derivatives. The apparent endothermic peak at 350 °C refers to the intramolecular dehydration of phosphoric acid [37], while the endothermic peak at 580 °C may be associated with the endothermic reaction between C and H_2O steam [33].

The egg-like morphology and high-porosity characterization of the reported PHPC-H and PHPC-W samples were identified by SEM and TEM techniques. As shown in Fig. 3 a and b, typical SEM images of PHPC-W and PHPC-H provide a direct proof for egg-like structure inheriting from the shape of bubbles formed during microwave irradiating or traditional heating process. Meanwhile, some small hollow carbon “eggs” aggregate to form larger “eggs” as exhibited in Figs. 1 and 3a. The typical TEM images of PHPC-W and PHPC-H, as shown in Fig. 3c and d, reveal the high-porosity nature and hollow egg-like structure. Meanwhile, a similar egg-like morphology is observed for PHPC-W fabricated by microwave irradiation under air atmosphere and PHPC-H fabricated by traditional pyrolytic carbonization under an inert atmosphere protection, indicating a negligible effect of carbonization method for morphology of the fabricated samples, but microwave heating completes the carbonization process in 1–5 min under ambient atmosphere, exhibiting impressive high efficiency and energy saving. The N_2 adsorption/desorption isotherms (Fig. 3e) and pore size distributions curves (Fig. 3f) of PHPC-W and PHPC-H series samples reveal the hierarchic porous nature of the fabricated samples. As shown in Fig. 3e, the similar isotherms are observed for PHPC-W and PHPC-H series samples although the carbonization method is very different. All of them exhibit an I/IV-type adsorption/desorption isotherms with an apparent hysteresis loop. A sharp rise of the N_2 isotherm at low relative pressure of less than 0.01 indicates developed microporosity, while a hysteresis loop ($0.6 < p/p_0 < 0.95$) suggests the existence of mesopores in the samples [9,26]. Meanwhile, the obvious rise of adsorption amount at high relative pressure ($p/p_0 > 0.97$) denotes the formation of macropores within the fabricated samples [38,39]. The coexistence of micropores, mesopores and macropores in the fabricated samples also is verified by pore size distributions curves. As shown in Fig. 3f, samples fabricated by microwave irradiation and traditional pyrolytic carbonization exhibit similar pore size distributions curves, and all of the micropores, mesopores and macropores can be identified. The micropores centered around at 0.64–0.66 and 0.78–0.80 nm are mainly caused by self-activating reaction between the sealed water steam in bubbles and carbon “egg-shell”, while the mesopores originate from the hollow egg-like structure, and macropores are mainly contributed by interstitial holes. Even so, the micropore and mesopore size of samples fabricated by microwave irradiation still slightly larger than that of PHPC-H. The details of the pore structures and specific surface area of the fabricated samples is presented in Table 1. As shown in Table 1, the specific surface area of the sample fabricated by microwave irradiation just for 1 min (PHPC-W_1) reaches 1194 $m^2\ g^{-1}$ with a pore volume of 1.62 $cm^3\ g^{-1}$, which sharply increases to 1642 $m^2\ g^{-1}$ when the microwave irradiating time increases to 3 min. It should be noted that the total surface area of mesopore and macropore decreases from 978 to 687 $m^2\ g^{-1}$ while the micropore surface area sharply increases from 215 $m^2\ g^{-1}$ to 955 $m^2\ g^{-1}$, the ratio of S_{mi}/S_{BET} dramatically increases from 0.18 to 0.58 as the microwave irradiating time increases from 1 to 3 min. As shown in Fig. 1, the micropores are mainly caused by activating reaction between the sealed water steam in bubbles and carbon “egg-shell”, the longer microwave irradiating time ensures the enough high reaction temperature and sufficient reaction time for this self-activating reaction. As the microwave irradiating time sequentially increases to 5 min, an apparent decrease for both total and micropore surface area is observed due to the drastic activating reaction under the sustained microwave irradiation which destroys the carbon wall of “egg-shell”. All of these results illuminate that microwave irradiation is a highly efficient and facile carbonization method, optimal morphology and textural parameters can be achieved in 3 min under air atmosphere using our suggested method. On the other hand, although the hierarchic porous carbons fabricated by microwave irradiation under air atmosphere and traditional pyrolytic carbonization under an inert atmosphere protection display similar morphology and pore size distributions, the PHPC-W sample fabricated under optimum condition exhibits a higher specific surface area and larger pore volume than that of PHPC-H. As shown in Table 1, the specific surface area and pore volume of PHPC-H only reach 1314 $m^2\ g^{-1}$ and 1.52 $cm^3\ g^{-1}$, respectively. A close value of the t-plot external surface area (total surface area of mesopores and macropores) is observed for PHPC-W_3 (687 $m^2\ g^{-1}$) and PHPC-H (632 $m^2\ g^{-1}$), but PHPC-W_3 exhibits more developed microporosity, which micropore surface area and pore volume are found to be far higher than that of PHPC-H. The larger specific surface area and pore volume of PHPC-W_3 may be due to ultra-fast heating and carbonization rate under microwave irradiation which induces more water is sealed in bubbles, and further reacts with the carbon “egg-shell” to form more developed microporosity. These results illuminate that microwave irradiation is a highly energy-efficient method comparing with the traditional pyrolytic carbonization method.

Fig. 4 presents the Raman spectrum of the fabricated samples. As shown in Fig. 4, all of the fabricated samples display two distinctive peaks at around 1350 and 1595 cm^{-1}, corresponding D- and G-band of carbon materials, respectively [40]. The G-band peak reflects the graphitic structure of sp^2 hybridized carbon atom bonded to adjacent C or P atoms, while the D-band peak corresponds to the disordered structure caused by defects in carbon lattice [41,42]. Thus, the intensity ratio of G-band and D-band (I_G/I_D) is commonly used to characterize the graphitization degree of carbon material. As shown in Fig. 4, the I_G/I_D ratio of the PHPC-W_1 only reaches 0.18 under microwave irradiation for 1 min, indicating an unsatisfactory graphitization degree due to insufficient irradiating time. As the microwave irradiating time increases

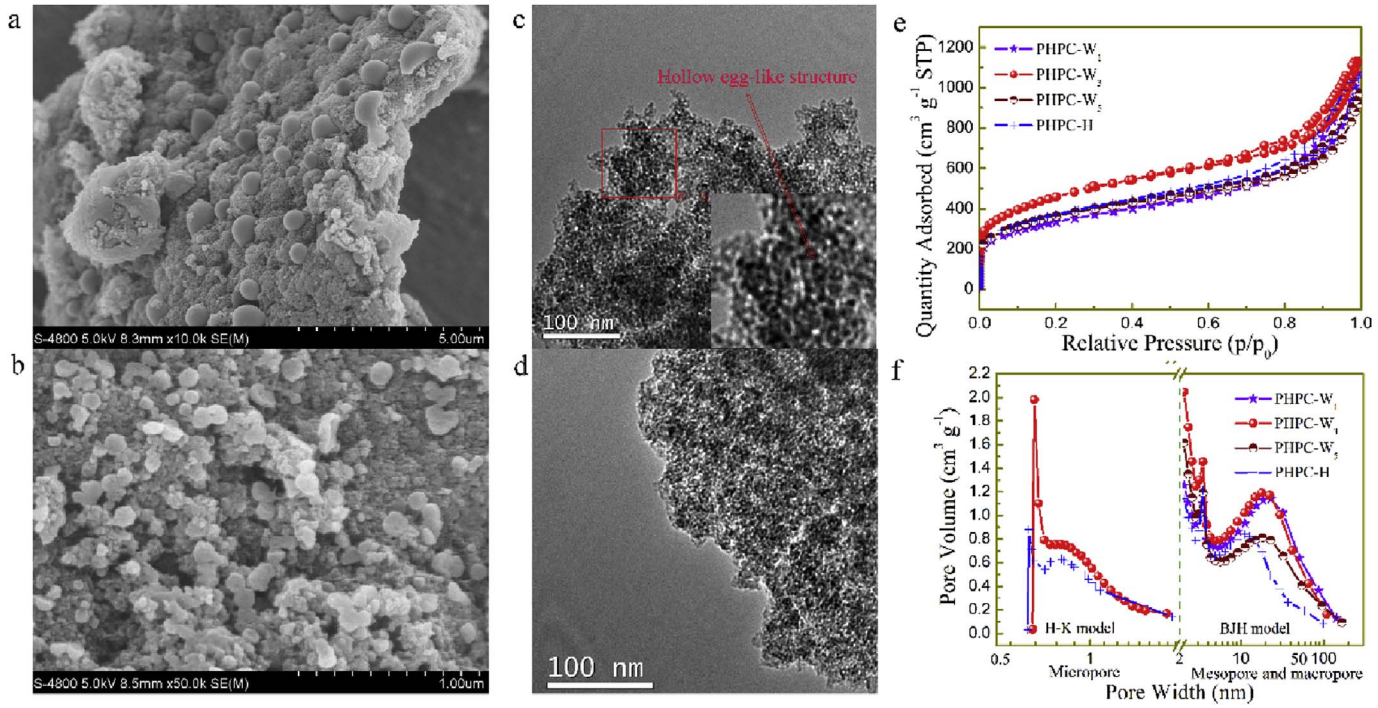

Fig. 3. Typiacal SEM images of PHPC-W (a) and PHPC-H (b); TEM images of PHPC-W (c) and PHPC-H (d); nitrogen adsorption/desorption isotherms (e) and pore size distributions cuvers (f) of the fabricated samples.

Table 1
Textural parameters of the fabricated samples.

Sample ID	$S_{BET}/m^2 g^{-1}$	$S_{me,\ ma}/m^2 g^{-1}$	$S_{mi}/m^2 g^{-1}$	S_{mi}/S_{BET}	$V_t/cm^3 g^{-1}$	$V_{mi}/cm^3 g^{-1}$
PHPC-W_1	1194	978	215	0.18	1.62	0.09
PHPC-W_3	1642	687	955	0.58	2.04	0.42
PHPC-W_5	1303	1089	214	0.16	1.33	0.08
PHPC-H	1314	632	682	0.52	1.52	0.31

S_{BET}: total surface area, $S_{me,\ ma}$: total surface area of mesopore and macropore, S_{mi}: micropore surface area, V_t: total pore volume, V_{mi}: micropore pore volume.

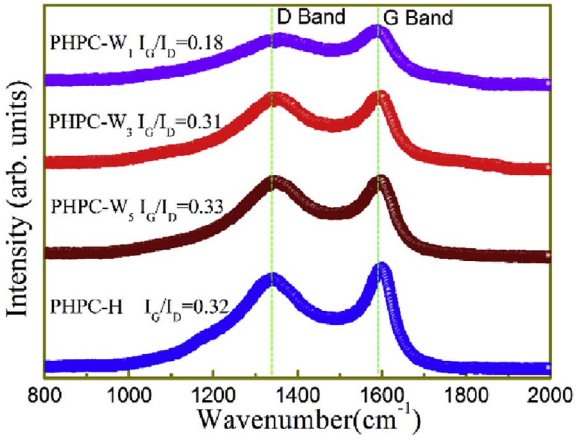

Fig. 4. Raman spectrum of the fabricated samples.

to 3 min, the I_G/I_D ratio sharply improves to 0.31, and then only a slight increase is observed when microwave irradiating time further increases to 5 min, illuminating that 3 min is an optimal microwave irradiating time again. Meanwhile, the I_G/I_D ratio of the sample fabricated at 650 °C under argon atmosphere for 2 h reaches 0.32, which value is very close to that of the PHPC-W_3 and PHPC-W_5, revealing that the similar graphitization degree with the sample fabricated by traditional pyrolytic carbonization under argon atmosphere for 2 h can be easily achieved by microwave irradiation only for 3–5 min under air atmosphere.

The element composition of the fabricated samples was analyzed by XPS, and the results are listed in Table 2. As shown in Table 2, carbon still is the dominant element for all samples. Beside the carbon, reasonable amounts of oxygen and phosphorus elements are detected. The oxygen element content of the samples PHPC-W_1, PHPC-W_3, and PHPC-W_5 reaches 13.60, 13.08 and 13.54 at. %, respectively, only a slight variation is observed with the increasing microwave irradiating time. Interestingly, the oxygen element content of PHPC-H fabricated under inert atmosphere protection arrives 14.44 at. %, which is higher than that of the PHPC-W series samples fabricated under air atmosphere, illuminating the incomparable advantage of our suggested method than that of traditional pyrolytic carbonization. The inert atmosphere absent fabrication process may be due to two reasons: 1) the ultra-fast carbonization process under microwave irradiation marvelously shorts the contact time of precursor with air; 2) the carbonization product is coated by highly thermostable phosphoric acid and its derivatives,

Table 2
Summary of XPS peak analysis on the fabricated samples.

Samples		PHPC-W_1	PHPC-W_3	PHPC-W_5	PHPC-H
C1s	**Content**	**83.47 at. %**	**85.40 at. %**	**85.96 at. %**	**83.02 at. %**
	284.5eV	69.7%	63.2%	63.3%	67.30%
	285.4eV	14.3%	21.3%	14.7%	20.20%
	286.5eV	16.0%	9.4%	15.6%	7.30%
	289.3eV	0.0%	6.1%	6.4%	5.20%
O1s	**Content**	**13.60 at. %**	**13.08 at. %**	**13.54 at. %**	**14.44 at. %**
	531.6 eV	24.7%	35.9%	23.3%	13.7%
	532.7 eV	9.7%	30.0%	11.8%	45.3%
	533.7 eV	65.6%	34.1%	64.9%	41.0%
P2p	**Content**	**2.93 at. %**	**1.52 at. %**	**1.50 at. %**	**2.54 at. %**
	132.6 eV	80.5%	65.5%	50.8%	58.0%
	134.2 eV	19.5%	34.5%	49.2%	42.0%

which avoids the direct contact of carbonization product with air. For phosphorus element, which content decreases from 2.93 to 1.52 at. % as the microwave irradiating time increases from 1 to 3 min, and only a slight reduction is observed as the microwave irradiating time sequentially increases to 5 min. Meanwhile, the phosphorus element content of the PHPC-H achieves 2.54 at. %, which value is slightly lower than that of PHPC-W_1, but far higher than that of PHPC-W_3 and PHPC-W_5, which may be due to the higher carbonization temperature for PHPC-W_3 and PHPC-W_5. In our experiment, a household microwave oven was used for fabricating PHPC-W series sample, so it was difficult to control the carbonization temperature. However, the phosphoric acid and its derivatives generated by decomposing of phytic acid and further condensation polymerization under microwave irradiation exhibit high thermostability, and can be heated by microwave irradiation to over 800 °C [37]. So, the carbonization temperature under microwave irradiation could reach over 800 °C in theory. The higher carbonization temperature caused by lasting microwave irradiation induces more serious pyrolysis of P-C and P═O bond, and thus causes an apparent decrease for phosphorus element content.

The incorporation of phosphorus heteroatoms into carbon lattice of the fabricated samples is confirmed by high-resolution XPS spectra of P2p orbit. As shown Fig. 5, two featured peaks at 132.6 eV and 134.2 eV attributing to P-C and P═O bonds respectively are observed for both PHPC-H and PHPC-W series samples [15,41]. The presence of P-C bonds verifies the successful doping of phosphorus heteroatoms into carbon lattice. Meanwhile, the relative content of P-C bonds for PHPC-W_1 and PHPC-W_3 reaches 80.5 and 65.5%, respectively, which values are higher than that of PHPC-H (58.0%), indicating the carbon atoms in graphite lattice can be more easily replaced by phosphorus heteroatoms under microwave irradiation than traditional pyrolytic carbonization (as shown in Table 2). Even so, the relative content of P-C bonds constantly decreases while the relative content of P═O bonds continually improves with the increasing microwave irradiating time. That results may be due to the higher bond energy of P═O bonds than that of P-C bonds, which makes the P-C bonds easier to decompose than P═O bonds under high temperature caused by microwave irradiation. For O1s orbit, three peaks centered at 531.6, 532.7, and 533.7 eV can be recognized for all samples. The peak at 531.6 ev corresponds to oxygen double bonded to carbon (C═O) in quinone type groups or phosphorus (P═O) in the phosphate group, while the peak at 532.7 eV refers to singly bonded oxygen (-*O*-) in C-O and C-*O*-P groups [43,44], the peak at 533.7 eV is attributed to O═C-O in carboxyl type groups [45]. It can be seen from Table 2, the PHPC-W series samples exhibit higher relative content of oxygen double bonded to carbon or phosphorus than that of PHPC-H (13.66%). It was reported that the pseudo-capacitance of carbon materials mainly originates from quinone − hydroquinone transitions [46,47], thus the higher relative content of quinone-type groups indicates a superior supercapacitance performance of PHPC-W than PHPC-H. In case of C1s orbit, the high-resolution spectra of C1s orbit for all samples exhibits four individual component peaks around 284.5, 285.4, 286.5 and 289.3 eV, which are attributed to graphitic structure (C-C sp^2), carbon-carbon single bonds of defects (C-C sp^3) or carbon-phosphorus single bonds (C-P) on the carbon matrix, carbon-oxygen-phosphorus single bonds (C-*O*-P) and carbon-oxygen double bonds (O-C═O), respectively [43,48]. O1s and C1s spectra confirm the presence of P═O and P-C bonds, which are in good agreement with the results of P2p spectrum.

Two-electrode coin-type symmetric supercapacitor cells using PHPC-H and PHPC-W series samples as electrodes were assembled to evaluate the capacitive performance of the reported samples (denoted as SC-PHPC-H and SC-PHPC-W_x, respectively). For comparing capacitive performance with commercial supercapacitor, a commercial activated carbon (AC) with a specific surface area of 1687 $m^2\ g^{-1}$ also was used to assemble coin-type symmetric supercapacitor cell (denoted as SC-AC). Fig. 6a presents cyclic voltammetry curves (CVs) of all test cells at a scan rate of 5 mV s^{-1}. As shown in Fig. 6a, cyclic voltammetry (CV) curves of all test cells exhibit good symmetrically rectangular shape, illuminating ideal electrochemical capacitance properties. The similar CV curves are observed for all test cells, but the covered area of CV curves for SC-PHPC-W_1, SC-PHPC-W_3 and SC-PHPC-W_5 is far larger than that of SC-AC and SC-PHPC-H, indicating the larger charge storage capability for the samples fabricated by microwave irradiation. In addition, the coved area of CV curves for SC-PHPC-W_x series cells proportionally rises with increasing scan rate, and the rectangular shape is well retained even under a large scan rate of 200 mv s^{-1} (as presented in Fig. S1 in the Supporting Information), suggesting a good ions transport ability and rate capability of the corresponding electrode material. The perfect triangular charge/discharge curves and nearly 100% coulombic efficiency under a current density of 0.5 A g^{-1} illuminate the ideal electrochemical capacitance properties of all test cells again (as shown in Fig 6b and Fig. S2). Low equivalent series resistance (ESR) for test cells is proved by their low IR drop (voltage drop). As shown in Fig. S3, only ca. 2.1 mV IR drop is observed for the typical cell SC-PHPC-W_3 under a current density of 0.5 A g^{-1}, and which value slowly rises to 34 mV as current density increases to 20 A g^{-1}.

The specific discharge capacitance (F g^{-1}) of single electrode for supercapacitor can be calculated by following equation:

$$C = \frac{4(I \times \Delta t)}{\Delta V \times m} \quad (2)$$

where C is the gravimetric specific capacitance of single electrode, I refers the applied discharge current (A), Δt and ΔV represent the discharging time (s) and potential range after the IR drop (V), respectively, and m (g) is the total mass of electrodes. At a current density of 0.5 A g^{-1}, single electrode specific capacitance of the PHPC-W series samples are calculated to be 192, 209 and 201 F g^{-1} for PHPC-W_1, PHPC-W_3 and PHPC-W_5, respectively. Unsurprisingly, the sample fabricated by microwave irradiation for 3 min (PHPC-W_3) with largest specific surface area exhibit a largest specific capacitance. Meanwhile, the single electrode specific capacitance of the PHPC-H and commercial AC only reaches 132 and 151 F g^{-1}, respectively. It should be noted that the sample PHPC-W_3 exhibits a similar specific surface area with the commercial AC, but the specific capacitance of the PHPC-W_3 is 1.4 times higher than that of commercial AC. The superior charge storage capability of PHPC-W series samples than that of commercial AC is mainly due to its unique structure and high electrolyte-accessible surface area. PHPC-W shows a hierarchic porous structure with short opened micropores (as shown in Figs. 1 and 3), while the closed micropore is dominated pore structure for commercial AC. It has been proved that the closed micropores with a pore size of less than 1 nm had a poor charge storage capability, but a mark charge storage capability can be harvested by short opened micropores due to the improved electrolyte accessibility [23,25]. The electrolyte accessibility of micropores is further enhanced by phosphorus heteroatoms doping. Incorporating phosphorus heteroatoms into carbon lattice greatly affects the physical and chemical properties of the carbon matrix. The difference in electronegativity of phosphorus and carbon atoms destroys the electro-neutrality of carbon lattice, and provides a more polarized surface, which enhances the surface wettability of carbon matrix and ensures a fast transfer rate of electrolytic ions in microporous and small mesoporous, improves the utilization ratio of specific surface and thus results in large specific capacitance [28,41,49]. A marked improvement for charge storage capability of PHPC-W series samples fabricated by microwave irradiation than that of PHPC-H fabricated by traditional pyrolytic carbonization also can be observed, as shown Table 1, the sample PHPC-W_5 exhibits a nearly similar specific surface area (1303 $m^2\ g^{-1}$) with the PHPC-H (1314 $m^2\ g^{-1}$), but the specific capacitance of PHPC-W_5 is about 1.5 times higher than that of PHPC-H. The larger charge storage capability for PHPC-W series samples is mainly contributed by the pseudo-capacitance. To confirm the contribution of pseudo-capacitance, the cyclic voltammetry (CV) of the fabricated samples were also tested in a three-electrode system at a scan

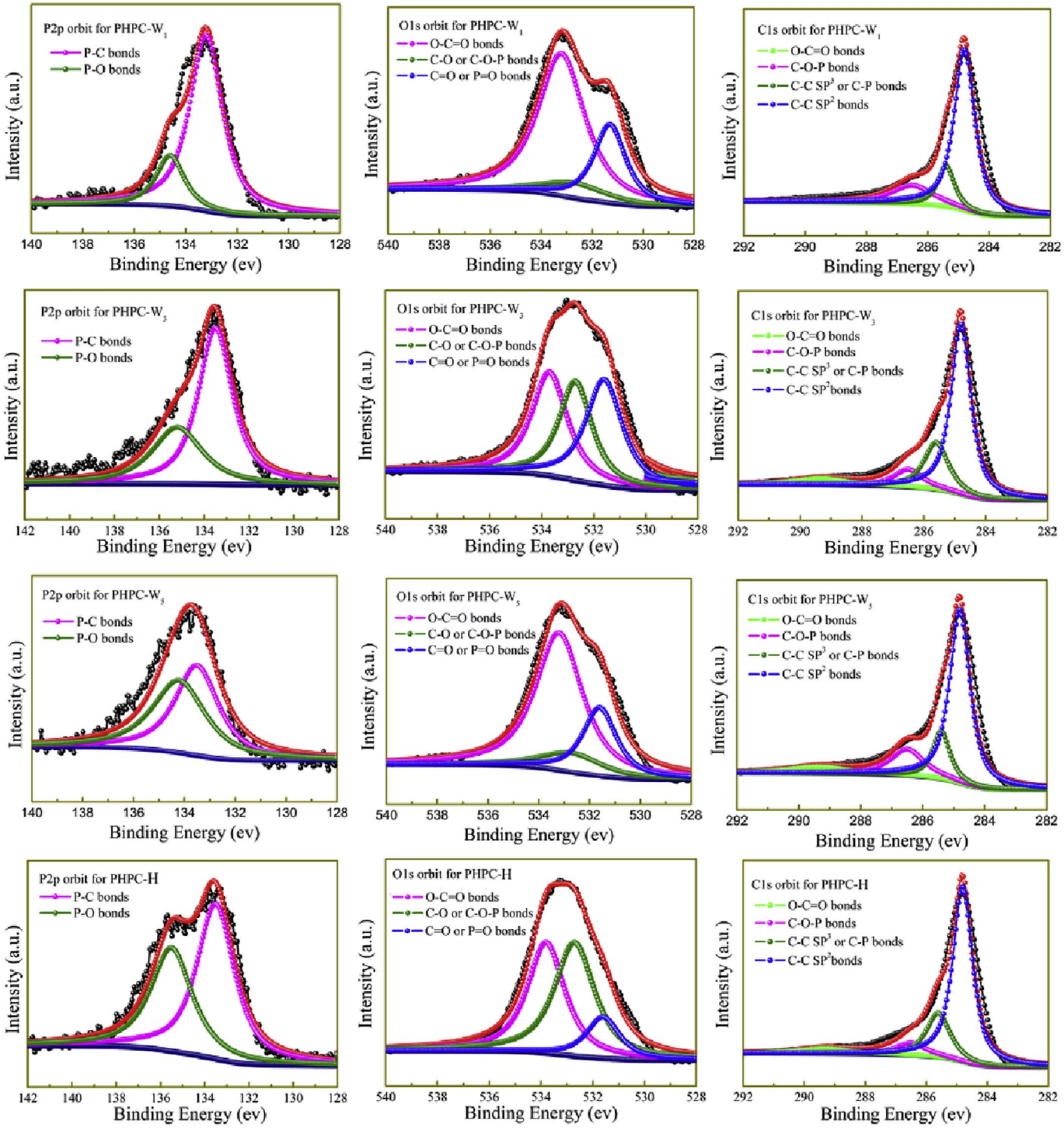

Fig. 5. High-resolution XPS spectra of P2p, O1s and C1s orbits for the fabricated samples.

rate of 5 mV s^{-1} in 6 M KOH. In common sense, the quasi-rectangular CV shape is a typical characteristic of electrical double-layer capacitance (EDLC) and the reversible redox peak always indicates the presence of pseudo-capacitance associated with fast and reversible oxidation/reduction (redox) or faradaic charge transfer reactions [50]. As shown in Fig. S4, the quasi-rectangular CV shape of the PHPC-H indicates the EDLC nature of the sample fabricated by traditional pyrolytic carbonization. But for PHPC-W series samples, a couple of apparent hump peaks overlapped on a quasi-rectangular CV shape are observed clearly for all samples, illuminating the contribution of pseudo-capacitance for the high charge storage capability of the samples fabricated by microwave irradiation. It was reported that the hump peaks on CV curve of carbon materials corresponds to the pseudo-capacitance inducing by quinone−hydroquinone transitions [46,47]. As shown in Fig. 5 and Table 2, although PHPC-H exhibits a slightly higher oxygen element content than that of the PHPC-W series samples, the relative content of the quinone-type groups on surface for PHPC-H is far lower than that of the PHPC-W series samples. To further confirm the origin of pseudo-capacitance, the sample of PHPC-W_5 was calcined at 650 °C for 2 h under argon atmosphere (named PHPC-W_5-H). As shown in Fig. S5 and Table S1, after calcining at 650 °C, no apparent variation for O content is observed, but the relative content of quinone-

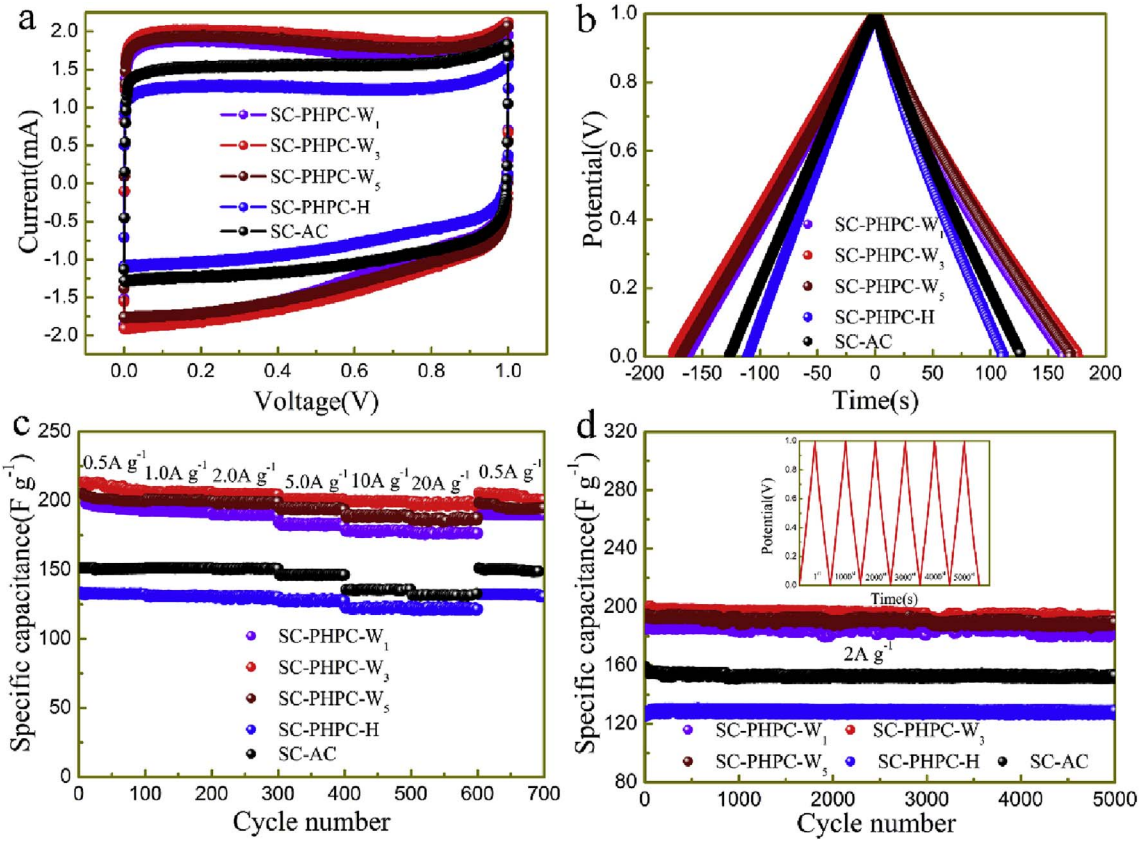

Fig. 6. The CV curves of the fabricated cells at a scan rate of 5 mV s^{-1} (a); galvanostatic charge–discharge curves of the fabricated cells under a current density of 0.5 A g^{-1} (b); rate capability of the fabricated electrodes (c); the cycling performance of the fabricated electrodes at the current density of 2 A g^{-1} (d); and galvanostatic charge/discharge curves of PHPC-W_3 electrode at 1st, 1000st, 2000st, 3000st,4000st and 5000st cycles (illustration in Fig. 6d).

type groups on surface reduces from 23.3% to 15.3%, the corresponding capacitance sharply decrease from 201 F g^{-1} to 154 F g^{-1}, which value is close to that of sample PHPC-H with a relative content of quinone-type groups about 13.7%. This result indicates that the pseudocapacitance on samples fabricated by microwave irradiation originates from high relative content of quinone-type groups on surface.

The fabricated PHPC-W series samples exhibit an extraordinary rate capability. As shown in Fig. 6c, the specific capacitance of PHPC-W series samples slowly reduces from 192, 209 and 201 F g^{-1} to 177, 201 and 191 F g^{-1} when current density increases from 0.5 to 20 A g^{-1} for PHPC-W_1, PHPC-W_3 and PHPC-W_5, respectively. The corresponding capacitance retention achieves 92.2, 96.2 and 95.0%, respectively, while that of PHPC-H and commercial AC only reaches 91.8% and 87.1%. The rate capability of PHPC-W series samples is superior to PHPC-H, commercial AC and other porous carbon materials reported in recent literatures [25,39,51–54]. The extraordinary rate capability of PHPC-W series samples maybe contributed by the hierarchic porous structure and enhanced surface wettability by phosphorus heteroatoms doping. Meanwhile, an excellent satisfying cycle stability for PHPC-W series samples is revealed by Fig. 6d. As shown in Fig. 6d, the capacitance retention rate reaches 95.3, 97.9 and 97.2% for PHPC-W_1, PHPC-W_3 and PHPC-W_5 respectively after 5000 times charge/discharge cycles, which values for PHPC-H and commercial AC are 94.96 and 92.4%, respectively. The high structure stability and unique morphology make a contribution for the excellent cycle performance of PHPC-W. As shown in Fig. 7, the CV curves before and after 5000 cycles for typical sample PHPC-W_3 are almost fully overlapped except a faint decay in plateau current for the latter, evidencing the excellent structure stability of PHPC-W series samples.

To further understand the electrochemical properties of the assembled supercapacitor cells, the EIS of the SC-PHPC-H and SC-PHPC-

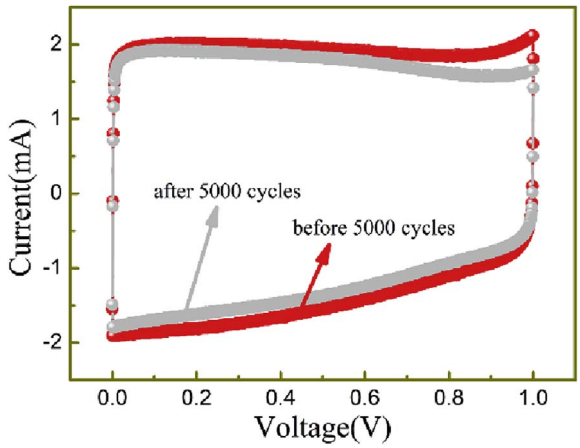

Fig. 7. CV curves of SC-PHPC-W_3 cell recorded before and after 5000 cycles.

W series cells were measured to compare the electrical resistances and ion transport behaviors. As shown in Fig. 8, almost vertical curves of Nyquist plots in low frequency for all test cells represent their nearly ideal capacitance behaviors, owing to developed porous structure and high electrolyte-accessible surface area [13]. The intercept at the real axis at high frequency region represents the equivalent series resistance [26], reflecting electrical conductivity of test electrodes. A good electrical conductivity for all samples is illuminated by low equivalent series resistance. As shown in Fig. 8, the equivalent series resistance for SC-PHPC-W_1, SC-PHPC-W_3, SC-PHPC-W_5 and SC-PHPC-H, is about 0.598, 0.584, 0.477 and 0.453 Ω, respectively. The equivalent series resistance decreases with the increasing microwave irradiating time due to the continually improving graphitization degree for PHPC-W

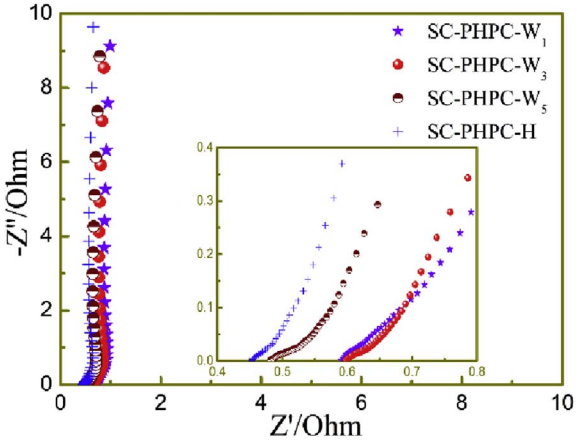

Fig. 8. Nyquist plots of the fabricated samples.

series samples (as shown in Fig. 4). For practical application, it is important to evaluate the leakage current and self-discharge characteristics of supercapacitor cells. As shown in Fig. S6, the leakage current of typical cell SC-PHPC-W_3 quickly stabilized at 0.043 mA, indicating a small leakage current and high stability for SC-PHPC-W series cells. After being charged at 1.0 V for 30 min, the open-circuit voltage of the SC-PHPC-W_3 and SC-PHPC-H cells exhibits a rapid decrease in the first hour and gradually stabilized at 0.69 and 0.55 V after 24 h, respectively, revealing their low self-discharge characteristic.

4. Conclusions

A phosphorus doped egg-like hierarchic porous carbon with superior supercapacitance performance was successfully fabricated by an ultra-facile and energy-efficient microwave irradiation combining with self-activation strategy. The similar morphology and graphitization degree with the sample fabricated by the traditional pyrolytic carbonization method under inert atmosphere protection for 2 h (PHPC-H) can easily achieves just for 3 min by the reported method. The samples fabricated by the reported method exhibit a unique phosphorus doped egg-like hierarchic porous structure with opened micropores, which specific surface area and pore volume achieves up to 1642 $m^2\ g^{-1}$ and 2.04 $cm^3\ g^{-1}$, respectively. The fabricated PHPC-W series samples exhibit a large charge storage capability and extraordinary rate capability, which specific capacitance reaches up to 209 F g^{-1} at a current density of 0.5 A g^{-1}, and more than 96.2% of initial capacitance is retained as the current density increasing to 20 A g^{-1}. Meanwhile, the capacitance retention rate of the PHPC-W series samples reaches up to 97.9% after 5000 times charge/discharge cycles. The hierarchic porous structure with developed opened microporosity, high electrolyte-accessible surface area and high conductivity contribute to the superior capacitance performance of the fabricated PHPC-W series samples. Comparing with the traditional pyrolytic carbonization method, the suggested microwave irradiation combining with self-activation strategy exhibits incomparable merits, such as high energy utilization efficiency, absence of inert atmosphere protection and ultra-fast fabrication process.

Acknowledgment

This work was supported by the National Natural Science Foundation of China (Grant No. 51462020 and 201664009), the Key Laboratory of Eco-Environment-Related Polymer Materials of the Ministry of Education Program (Grant No. KF-13-01), the Foundation for Innovation Groups of Basic Research in Gansu Province (Grant No. 1606RJIA322).

Appendix A. Supplementary data

Supplementary data related to this article can be found at http://dx.doi.org/10.1016/j.jpowsour.2017.10.082.

References

[1] X.Y. Xiao, Y.C. Li, Z.P. Liu, Nat. Mater. 15 (2016) 697–698.
[2] S. Park, Nat. Rev.Mater. 1 (2016) 16085.
[3] C.J. Chen, Y. Zhang, Y.J. Li, J.Q. Dai, J.W. Song, Y.G. Yao, Y.H. Gong, I. Kierzewski, J. Xie, L.B. Hu, Energ. Environ. Sci. 10 (2017) 538–545.
[4] Q. Wang, J. Yan, Z.J. Fan, Energ. Environ. Sci. 9 (2016) 729–762.
[5] M. Sevilla, R. Mokaya, Energ. Environ. Sci. 7 (2014) 1250–1280.
[6] J.H. Hou, C.B. Cao, F. Idrees, X.L. Ma, ACS. Nano 9 (2015) 2556–2564.
[7] M.J. Jing, Y.C. Yang, Y.R. Zhu, H.S. Hou, Z.B. Wu, X.B. Ji, Electrochim. Acta 141 (2014) 234–240.
[8] D.S. Yu, K. Goh, H. Wang, L. Wei, W.C. Jiang, Q. Zhang, L.M. Dai, Y. Chen, Nat. Nano 9 (2014) 555–562.
[9] P. Hao, Z.H. Zhao, Y.H. Leng, J. Tian, Y.H. Sang, R.I. Boughton, C.P. Wong, H. Liu, B. Yang, Nano. Energy 15 (2015) 9–23.
[10] B. Li, F. Dai, Q.F. Xiao, L. Yang, J.M. Shen, C.M. Zhang, M. Cai, Adv. Energy. Mater. 6 (2016) 1600802-n/a.
[11] D.M. Kang, Q.L. Liu, J.J. Gu, Y.S. Su, W. Zhang, D. Zhang, ACS. Nano 9 (2015) 11225–11233.
[12] J.K. Ou, L. Yang, Z. Zhang, X.H. Xi, J. Power Sources 333 (2016) 193–202.
[13] X.Y. Li, K.T. Liu, Z.Z. Liu, Z.B. Wang, B. Li, D.L. Zhang, Electrochim. Acta 240 (2017) 43–52.
[14] E.Y.L. Teo, L. Muniandy, E.P. Ng, F. Adam, A.R. Mohamed, R. Jose, K.F. Chong, Electrochim. Acta 192 (2016) 110–119.
[15] U.B. Nasini, V.G. Bairi, S.K. Ramasahayam, S.E. Bourdo, T. Viswanathan, A.U. Shaikh, J. Power Sources 250 (2014) 257–265.
[16] E.G. Calvo, N. Ferrera-Lorenzo, J.A. Menéndez, A. Arenillas, Microporous Mesoporous Mater. 168 (2013) 206–212.
[17] A.M. Schwenke, S. Hoeppener, U.S. Schubert, Adv. Mater. 27 (2015) 4113–4141.
[18] K.Y. Foo, B.H. Hameed, Microporous Mesoporous Mater. 148 (2012) 191–195.
[19] K. Yang, J. Peng, C. Srinivasakannan, L. Zhang, H. Xia, X. Duan, Bioresour. Technol. 101 (2010) 6163–6169.
[20] C. Saucier, M.A. Adebayo, E.C. Lima, R. Cataluña, P.S. Thue, L.D.T. Prola, M.J. Puchana-Rosero, F.M. Machado, F.A. Pavan, G.L. Dotto, J. Hazard. Mater. 289 (2015) 18–27.
[21] U.B. Nasini, V. Gopal Bairi, S. Kumar Ramasahayam, S.E. Bourdo, T. Viswanathan, A.U. Shaikh, ChemElectroChem 1 (2014) 573–579.
[22] L.L. Zhang, X.S. Zhao, Chem. Soc. Rev. 38 (2009) 2520–2531.
[23] J. Chmiola, G. Yushin, Y. Gogotsi, C. Portet, P. Simon, P.L. Taberna, Science 313 (2006) 1760–1763.
[24] M.H. Sun, S.Z. Huang, L.H. Chen, Y. Li, X.Y. Yang, Z.Y. Yuan, B.L. Su, Chem. Soc. Rev. 45 (2016) 3479–3563.
[25] D.Y. Zhang, M. Han, B. Wang, Y.B. Li, L.Y. Lei, K.J. Wang, Y. Wang, L. Zhang, H.X. Feng, J. Power Sources 358 (2017) 112–120.
[26] L. Xie, G. Sun, F. Su, X. Guo, Q. Kong, X. Li, X. Huang, L. Wan, W. song, K. Li, C. Lv, C.M. Chen, J. Mater. Chem. A 4 (2016) 1637–1646.
[27] D.Y. Zhang, Y. Hao, L.W. Zheng, Y. Ma, H.X. Feng, H.M. Luo, J. Mater. Chem. A 1 (2013) 7584–7591.
[28] D.Y. Zhang, M. Han, Y.B. Li, L.Y. Lei, Y.H. Shang, K.J. Wang, Y. Wang, Z.K. Zhang, X.D. Zhang, H.X. Feng, Electrochim. Acta 222 (2016) 141–148.
[29] S. Faraji, F.N. Ani, J. Power Sources 263 (2014) 338–360.
[30] G. Jiang, J. Qiao, F. Hong, Int. J. Hydrogen Energ 37 (2012) 9182–9192.
[31] C. Cheng, J. Zhang, Y. Mu, J. Gao, Y. Feng, H. Liu, Z. Guo, C. Zhang, J. Anal. Appl. Pyrolysis 108 (2014) 41–46.
[32] D. Montané, V. Torné-Fernández, V. Fierro, Chem. Eng. J. 106 (2005) 1–12.
[33] Z.Y. Sui, Q.H. Meng, J.T. Li, J.H. Zhu, Y. Cui, B.H. Han, J. Mater. Chem. A 2 (2014) 9891–9898.
[34] Q. Zhao, Y. Zhang, Y. Meng, Y. Wang, J. Ou, Y. Guo, D. Xiao, Nano Energy 34 (2017) 408–420.
[35] E.O. Silva, A.P.F.R.L. Bracarense, J. Food Sci. 81 (2016) R1357–R1362.
[36] J.C. Ojeda Toro, I. Dobrosz-Gómez, M.Á. Gómez García, AIChE J. 62 (2016) 4418–4426.
[37] M.A. Nahil, P.T. Williams, Biomass Bioenergy 37 (2012) 142–149.
[38] T. Yang, R. Zhou, D.-W. Wang, S.P. Jiang, Y. Yamauchi, S.Z. Qiao, M.J. Monteiro, J. Liu, Chem. Commun. 51 (2015) 2518–2521.
[39] J. Zhao, H. Lai, Z. Lyu, Y. Jiang, K. Xie, X. Wang, Q. Wu, L. Yang, Z. Jin, Y. Ma, J. Liu, Z. Hu, Adv. Mater. 27 (2015) 3541–3545.
[40] D.S. Yang, D. Bhattacharjya, M.Y. Song, J.S. Yu, Carbon 67 (2014) 736–743.
[41] F. Razmjooei, K.P. Singh, M.Y. Song, J.S. Yu, Carbon 78 (2014) 257–267.
[42] K.L.Y.T. Liu, Y. Liu, L.T. Pu, Z.H. Chen, S.G. Deng, J. Mater. Chem. A 3 (2015) 21149–21158.
[43] L. Qie, W.M. Chen, H.H. Xu, X.Q. Xiong, Y. Jiang, F. Zou, X.L. Hu, Y. Xin, Z.L. Zhang, Y.H. Huang, Energ. Environ. Sci. 6 (2013) 2497–2504.
[44] Y. Wen, B. Wang, C. Huang, L. Wang, D. Hulicova-Jurcakova, Chem. Eur. J. 21 (2015) 80–85.
[45] J. Zhou, Z.S. Zhang, W. Xing, J. Yu, G.X. Han, W.J. Si, S.P. Zhuo, Electrochim. Acta 153 (2015) 68–75.
[46] K. Singh, M. Seredych, E.R. Castellon, T.J. Bandosz, ChemElectroChem 1 (2014) 565–572.

[47] D.Y. Zhang, L.W. Zheng, Y. Ma, L.Y. Lei, Q.L. Li, Y. Li, H.M. Luo, H.X. Feng, Y. Hao, ACS Appl. Mater. Interfaces 6 (2014) 2657–2665.
[48] Y. Zhou, R. Ma, S.L. Candelaria, J. Wang, Q. Liu, E. Uchaker, P. Li, Y. Chen, G. Cao, J. Power Sources 314 (2016) 39–48.
[49] X. Yu, Y. Kang, H.S. Park, Carbon 101 (2016) 49–56.
[50] D. Zhang, L. Lei, Y. Shang, K. Wang, Y. Wang, Appl. Surf. Sci. 360 (Part B) (2016) 807–815.
[51] K. Yuan, T. Hu, Y. Xu, R. Graf, G. Brunklaus, M. Forster, Y. Chen, U. Scherf, ChemElectroChem 3 (2016) 822–828.
[52] L.J. Zhang, Y.Z. Jiang, L.W. Wang, C. Zhang, S.X. Liu, Electrochim. Acta 196 (2016) 189–196.
[53] C. Ma, X.Y. Chen, D.H. Long, J.T. Wang, W.M. Qiao, L.C. Ling, Carbon 118 (2017) 699–708.
[54] K. Yuan, T. Hu, Y. Xu, R. Graf, L. Shi, M. Forster, T. Pichler, T. Riedl, Y. Chen, U. Scherf, Mater. Chem. Front. 1 (2017) 278–285.